Applications of Fiber Lasers for the Development of Compact Photonic Devices

Rose Mary, Debaditya Choudhury, *Member, IEEE*, and Ajoy K. Kar, *Member, IEEE*

(Invited Paper)

Abstract—Ultrafast fiber lasers, with their distinct features of high stability, superior beam quality, compactness and power scalability have revolutionized a variety of applications, ranging from micromachining and medical diagnostics to basic research. One of the applications include Ultrafast Laser Inscription, a technology that has considerably improved and diversified with advances in stable, high power Ytterbium-doped fiber lasers. This paper explores the highly interdisciplinary application realm of Ultrafast Laser Inscription for the development of novel photonic and optofluidic devices.

Index Terms—Fiber Lasers, laser applications, optical fiber applications, optical devices, optoelectronic devices.

I. INTRODUCTION

THE first fiber laser was demonstrated over 50 years ago by E. Snitzer in a Neodymium doped fiber [1], [2]. Today, fiber lasers find innumerable applications in a variety of fields ranging from medical diagnostics, laser material processing, imaging, metrology, and scientific research. It is interesting to note how advances in fiber optics have revolutionized laser technology; especially since at the inception of both these technologies, this was far from envisaged. Optical fiber technology was conceived as a superior alternative to conventional copper cables for telecommunication applications. With the manufacturing success in low-loss optical fibers complemented by the advent of high-brightness semiconductor diode lasers, communication systems based on optical fibers were realized with unprecedented advancement in terms of speed and data transmission capacity over long distances. Extensive research exploring further application potential of optical fibers grew only after this. Development of low-loss rare earth doped fibers in the 1980s led to the first reports of fiber lasers emitting output powers of the order of a few megawatts [3]. Since then, fiber laser technology has grown exponentially with average power outputs close to

kilowatt range [4], [5]. The unique advantages of fiber lasers over conventional solid state lasers have also led to their rapid commercialization.

The advancement in the field of fiber lasers can be attributed to certain defining features that arise due to their waveguide geometry. In fiber lasers, light is tightly confined to a small cross-sectional area, allowing high intensities within the core. Long lengths of the fiber can be used to obtain high gain, while still maintaining a rugged and compact cavity configuration. This makes these lasers highly stable. Another advantage is their ease of use. The laser beam delivery becomes inherently simple due to the fiber based configuration. The availability of high power laser diodes has allowed optical pumping of the system. Integrated cavities and all-fiber formats have become possible with the advent of fiber-coupled components and fiber Bragg gratings [6]. The high surface area to volume ratio in optical fibers allows excellent heat dissipation, facilitating unprecedented power scaling capacity. The high intensities in the fiber cores are however accompanied by undesirable nonlinear phenomena which results in power limitation, fiber facet damage [7], and fiber fuse effects [8]. The strength of the nonlinear effects depends on the intensity in the fiber core, and the interaction length. Considerable research has been undertaken with a view of overcoming these limitations for the optimization of fiber laser architectures. Examples include double-clad fiber design, and rare earth doped photonic crystal fibers [7].

The most common rare earth doped fiber lasers [9] use Ytterbium (Yb) and Erbium (Er) dopants, with their operating wavelength around 1.03 μm and 1.5 μm, respectively. Ytterbium doped systems have become increasingly popular over their Nd: doped bulk laser counterpart, due to the added advantages of low thermal load and the absence of fluorescence quenching. In fiber lasers, ultrafast operation is typically achieved by having an appropriate saturable absorber (SA), or by dispersion management in the system. In the latter case, Yb doped fiber lasers work in the normal dispersion regime and rely on nonlinear polarization evolution for self-starting mode-locking [10], [11]. Semiconductor Saturable Absorber Mirrors (SESAM) [12], popularly used for mode-locked operation in solid–state bulk lasers have also been used in fiber systems [13]. However, the use of SESAMs is not preferred since the fiber laser cavity design deters from being compact and alignment-free. The emergence of carbon nanotubes(CNT) and graphene as novel SAs have resulted in a new phase to the development of ultrafast lasers, including fiber lasers [14]. CNT and graphene have a broad operation wavelength, picosecond recovery times, and small modulation

R. Mary and A. K. Kar are with the Nonlinear Optics Group at Institute of Photonics and Quantum Sciences, Heriot-Watt University, Edinburgh EH14 4AS, U.K. (e-mail: rm330@hw.ac.uk; A.K.Kar@hw.ac.uk).

D. Choudhury is with the Photonics Instrumentation Group, Institute of Photonics and Quantum Sciences, Heriot-Watt University, Edinburgh EH14 4AS, UK (e-mail: D.Choudhury@hw.ac.uk).

depths, allowing relatively simple passive mode locking of fiber systems.

Fiber lasers are currently in use in a variety of application regimes. For micromachining, which predominantly used CO_2 lasers, fiber lasers emerged as a superior alternative with easy beam delivery and a robust setup. They are also less bulky and more convenient to use compared to CO_2 lasers, which use Helium gas in the system [15]. Consequently, micromachining has evolved at a rapid pace over the years, from hole drilling [16] and surface re-structuring [17] to fabrication of sub-micron features with high precision. Lasers have been used for micromachining both absorptive and transparent materials [18]. In this paper, we discuss the role played by fiber lasers in the field of micromachining of transparent materials. Laser micromachining in transparent dielectrics was first demonstrated in 1996 by Davis *et al.* [19]. They reported a permanent refractive index change within a bulk dielectric by tightly focusing femtosecond laser pulses within the material. The mechanisms of material modification has since been widely studied, and is attributed to the nonlinear excitation processes that occur as a result of the high intensities at the laser focus [18], [20], [21]. Modification in materials have been manifested in a number of forms including material ablation [22], bubble formation [23], voids [24], [25], nano cracks [21], [26] and refractive index change [24], [27]. The type of modification depends highly on the nature of the material, and the inscription laser parameters. This type of direct laser writing offers a number of advantages over conventional waveguide fabrication methods. It is a rapid process requiring no clean room facilities as needed for thin-film deposition techniques. The process can also be employed in a wide variety of materials including many glasses, crystals and ceramics that are transparent to the operating wavelength of the laser. However, the most distinct feature of this femtosecond laser based material processing is its three-dimensional (3-D) fabrication capability. Since the first demonstration, the technique has rapidly developed, emerging as a stand-alone technological field and known by various names. "Ultrafast Laser Inscription" (ULI), one of the nomenclature, also used throughout this paper, is now an established field and acknowledged as a powerful tool for novel photonic device fabrication. ULI is capable of impacting a variety of fields, including opto-fluidics [28], passive and active waveguide devices [29], [30] and micro-mechanics [31]. The repeatability and reliability of ULI devices have improved considerably with the use of robust fiber lasers.

Over the years, the number of materials viable for ULI has increased and the technology has been used for the fabrication of various devices including waveguide lasers [27], [30], and waveguide amplifiers [32]. The majority of the initial defining studies used regeneratively amplified Titanium doped Sapphire lasers at an operating wavelength of 800 nm, with pulse durations of about 100 fs, and kilohertz repetition rates. While these systems provide high pulse energies of the order of microjoules to millijoules, typical fabrication times were slow owing to the lower repetition rates. Titanium Sapphire oscillators, but with no amplifier stage, operating at megahertz repetition rates and low pulse energies have also been used. Currently, compact laser systems that are well-suited for industrial environments are
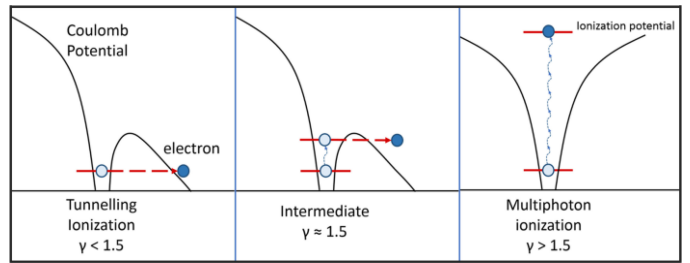

Fig. 1. Photo-ionization mechanisms and corresponding Keldysh parameter.

preferred for laser material processing, such as cavity dumped Yb:KYW oscillators [33]. Other laser systems of importance are high repetition rate Yb–doped fiber lasers (100 kHz–5 MHz), with high pulse energies of the order of nanojoules to microjoules. These systems have greatly reduced fabrication times for low-loss waveguides. Studies in the field of ULI spanning more than 15 years have now established optimized laser parameters associated with low-loss waveguide fabrication in a variety of materials. In this paper, we discuss the key aspects of ULI using a variable repetition rate Yb-doped IMRA fiber laser (IMRA FCPA μJewel D400). Even though ULI is fast becoming a well-documented field, this paper gives a brief description about the dynamics of energy transfer and types of material modification for completeness. The multidisciplinary impact of ULI in the fields of compact laser source development and optofluidic applications has been detailed.

II. MATERIAL MODIFICATION REGIMES

When an ultrashort laser pulse is focused within a dielectric material, the high peak irradiances of the order of 10 TW/cm^2 causes laser induced optical breakdown through a combination of photo-ionization and avalanche ionization processes.

In photo-ionization process, the energetic electrons in the valence band are promoted to the conduction band depending on the intensity and energy of the incident light, and can occur by two distinct methods, namely, multiphoton ionization and tunnelling ionization. In multiphoton ionization, electrons are released from the material by simultaneous absorption of two or more photons. Tunnelling ionization takes place when the input laser field is strong enough to distort the Coulomb field felt by the electron, allowing the electron to tunnel out of its bound state. A theoretical framework for these processes was put forward by Keldysh in 1964 [20] which introduced a parameter γ that determines the dominant photo-ionization process in a material. γ is known as the Keldysh parameter and is given by

$$\gamma = \frac{\omega}{e} \sqrt{\frac{mcn\varepsilon_0 E_g}{I}} \tag{1}$$

where ω is the laser frequency, c is the speed of light, n is the refractive index, ε_0 is the permittivity of free space, E_g is the band-gap of the material, I is the laser irradiance, and m and e are the reduced electron charge and mass. For multiphoton ionization, $\gamma > 1.5$ and when $\gamma < 1.5$, tunnelling ionization is predominant. When $\gamma = 1.5$, photo-ionization is a combination of multiphoton and tunnelling ionization processes. Fig. 1

depicts the occurrence of photo-ionization mechanisms with respect to the Keldysh parameter.

Avalanche ionization occurs when there are free electrons available in the material, which act as seed for the avalanche process. These electrons absorb the incident laser light and can thereby achieve a kinetic energy higher than the ionization potential of a bound electron. When such an energetic electron strikes the lattice, it can dislodge a bound electron resulting in two free electrons of lower energy. This process known as impact ionization gets repeated, creating an avalanche of electrons. This avalanche process results in plasma generation.

When the generated plasma reaches a critical density at which the plasma oscillation frequency equals the laser frequency, the material breaks down and becomes absorbing. The absorbed energy is transferred to the lattice, heating up the material. The dynamics of energy transfer depends mainly on the input laser pulse duration. At pulse energies greater than the damage threshold of the material, the heating effect results in damage structures and voids, often accompanied by refractive index changes around the structure. These refractive index changes occur due to induced stress around the damage. Refractive index changes are observed even at low pulse energies, where the plasma is not energetic enough to create ablations. Even though the science behind this mechanism is not fully understood, this regime is most used for the fabrication of optical waveguides; since it provides a specific path of isotropic refractive index modification. Thus, focused ultrafast laser pulses can create permanent modifications in a dielectric material, in the form of smooth structures with a refractive index change or at higher pulse energies, highly scattering nanostructures or voids. The modifications can be extended along any arbitrary path in 3 dimensions, usually by translating the substrate. The different modifications find different uses for various device architectures.

The realization of a desired modification involves a successful interplay of the determining parameters of the inscription laser, focusing optics, and the material under study. In terms of the laser properties, the pulse energy, repetition rate, laser wavelength, pulse duration and laser polarization play a vital role. Deterministic material features include bandgap energy, thermal and nonlinear properties, and material symmetry, in the case of crystals. Other factors include the numerical aperture of the lens, inscription geometry and translation speed. Some of the determining features will be described below.

The different useful material modification regimes tailored using ULI include smooth refractive index change, nanogratings, and void formation.

The homogeneous refractive index change occurs at laser pulse energies marginally higher than the material modification threshold. The refractive index can be positive or negative depending upon the material under study, with the change typically of the order of 10^{-3} [34]. For fused silica, the positive refractive index modification threshold is 50 nJ for $\sim$150 fs pulse durations [35]. The isotropic refractive index change is explained by different hypotheses, namely, thermal effects [36], [37], color center formation [19], [38] and structural change [27], [39]. However, these do not provide an explicit nor exhaustive under-

standing of the possible modifications, for instance, the possibility of both positive and negative refractive index in certain multicomponent glasses [40].

At laser pulse energies higher than that required for homogeneous refractive index change, self-organized nanogratings are formed. The formation depend strongly on the polarization of the incident pulse train, and the orientation of these well-defined, periodic structures are found to be orthogonal to the electric field vector of the laser beam. This structural modification is associated with interference between the incident laser field and the electric field of the free electron plasma wave in the material. ULI based nanogratings in fused silica are found to exhibit enhanced chemical etching properties in comparison to the unmodified material. This phenomena is beneficial for the fabrication of microfluidic elements.

When the intensity at the laser focus exceeds the ablation threshold of the material, the energy transfer of free electron plasma into the lattice is accompanied by the formation of pressure waves. These effects are manifested in the form of micro-explosions and void formation within the material.

The diverse regimes of material modification possible by ULI have been used for a variety of applications. For instance, the enhanced chemical etching sensitivity of nanogratings fabricated by ULI has a huge impact for optofluidic device applications. The void formation regime finds potential application for 3-D memory storage. Most popularly, ULI is used for waveguide inscription. Waveguide inscription studies have been reported in numerous materials including fused silica, borosilicate, phosphate, bismuthate chalcogenides, ceramics, and crystals including Nd: YAG, Yb:KYW, lithium niobate and KTP. This has led to classifications based on the type of waveguide morphology and corresponding modification regime. Consequently, ULI based waveguides can be broadly classified as Type I and Type II.

Type I waveguide inscription utilizes the smooth refractive index modification regime that occurs at low pulse energies. It is possible in most glass materials, and certain crystals and ceramics. The smooth refractive index maybe manifested in the form of positive or negative refractive index, or a combination of both. For materials that have a positive refractive index change by ULI, the modified region forms the core, while the surrounding unmodified region forms the cladding of the waveguide. Other novel inscription designs have allowed waveguide fabrication in materials that exhibit a negative refractive index change by ULI. These include double-cladding [41], and depressed cladding structures [42].

Type II inscription is essentially used in crystals, and materials in which smooth positive refractive index change is not achieveble. In this method, the ultrafast laser is used to inscribe two damage tracks in the material. The strained material within the damage lines undergoes a refractive index change due to the strain-optic effect, allowing light guidance through this region. This mode of inscription has few drawbacks compared to Type I, such as the unpredictable nature of the guiding regions, polarization dependence, and effect of the strain field from multiple damage tracks. This method has however been very effective for waveguide laser applications [43], [44].
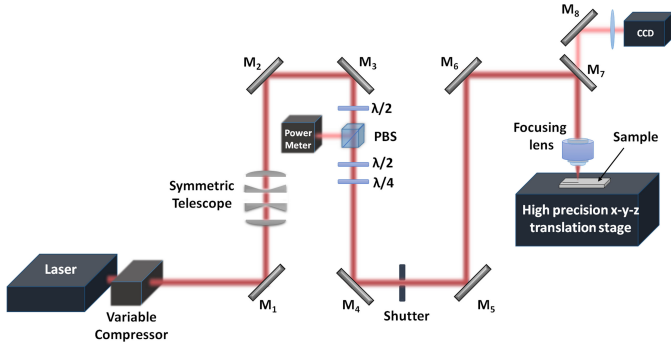
Fig. 2. ULI Setup- The IMRA inscription setup, with power control (λ/2 plate, PBS: Polarization Beam Splitter, and power meter), and polarization control (λ/2 plate and λ/4 plate)
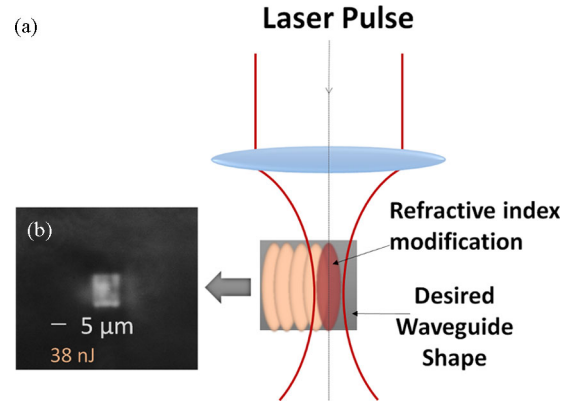

Fig. 3. (a) Schematic of the multi-scan waveguide fabrication. (b) The square waveguide cross-section achieved in Yb-doped Bismuthate glass at 38 nJ laser pulse energy, and 1 MHz repetition rate.

III. Ultrafast Laser Inscription Setup

The ULI setup used for the study discussed in this paper is given in Fig. 2. The laser system is a variable repetition rate Yb-doped fiber based master oscillator power amplifier system (IMRA FCPA μJewel D400). A pulse picker positioned before the power amplifier stage can vary the repetition rate between 100 kHz and 5 MHz. The laser system also includes an adjustable compressor that can be used to change the pulse duration. Therefore, the laser is capable of producing transform limited pulses with duration as low as 350 fs to longer, chirped pulses of 1–2 ps duration. The laser output is linearly polarized with the operating wavelength centered at 1047 nm. The output from the compressor stage is steered using mirrors M1-M3 and incident on a half-wave plate and a polarization beam splitter for a calibrated control of the average power. This is followed by optics for the polarization control of the beam; a half-wave plate to rotate the plane of polarization, and a quarter wave plate to attain circularly polarized pulses. The beam is subsequently steered using mirrors M4–M7 to a vibration insensitive granite gantry and aligned through the focusing optic onto the substrate for inscription. The substrate is placed on automated high-precision, air-bearing x–y–z translation stages (Aerotech).

The inscription geometry is an important factor for waveguide fabrication. In the transverse inscription geometry, the sample translation direction is maintained perpendicular to the beam propagation. The resultant material modification exhibits an asymmetric cross-section, the spatial distribution of which depends on the beam waist and the confocal parameter of the voxel created by the focused beam. The asymmetry is especially affected by the numerical aperture (NA) of the focusing lens. A variation in NA changes the confocal parameter faster than the beam waist. In comparison, the longitudinal inscription geometry involves the substrate translation along the same direction as the beam propagation and therefore allows the cross-section of the modified region to be defined by the symmetry of the beam itself. However, the working distance of the lens limits the translation distance, which consequently limits the lengths of the waveguides achievable using this geometry. In addition, for an inscription beam with Gaussian profile, increased spherical aberration with varying depths present a drawback in inscribing deeply embedded structures. However, inscription

of waveguides in this geometry using a non-diffracting Bessel beam has recently been demonstrated [45]. Various beam shaping techniques have been proposed to correct the asymmetry of waveguide cross-sections in the transverse inscription geometry, including astigmatic beam shaping technique [46], the slit technique [47], deformable mirror [48], adaptive optics [49] and multi-scan [50]. Therefore, the transverse geometry which provides a more flexible working range and 3-D capabilities is preferred in spite of the asymmetric waveguides; and is used for the study presented in this paper. We use the multi-scan technique, which is now established as a reliable method, in which the desired waveguide cross-section is tailored by multiple overlapping scans by the laser. The method employs consecutive scans with each scan offset by a small distance in a direction perpendicular to both the laser propagation direction and waveguide axis. This technique is independent of the intensity distribution at the focal region and provides waveguides with almost square cross-sections and a step index refractive index profile. The multi-scan technique provides an elegant method to independently control the size of the waveguide cross-section by varying the scan parameters and the change in refractive index by varying the translation speed, which is not possible using other cross-section shaping approaches. Fig. 3 shows a schematic diagram of the multi-scan fabrication technique and the corresponding optical micrograph image of the end facet of a waveguide fabricated in Yb-doped Bismuthate glass. This technique has been reported to produce waveguides with insertion losses as low as 0.12 dB cm^{-1}. An increase in the fabrication time is a disadvantage although it is possible to circumvent this by choosing appropriate writing parameters.

IV. ULI Applications

A. Compact Waveguide Laser Sources at 1 Micrometer

One of the widely explored applications of ULI includes the fabrication of optical amplifiers and lasers, by the inscription of waveguides within laser gain media, typically rare earth doped substrates [27], [30], [32], [51]–[53]. Successful mode-locking of waveguide lasers have also been reported [30], [54]. Rare
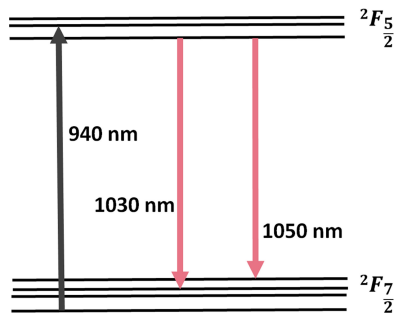
Fig. 4.   Energy level diagram of Yb^{3+} ions. The commonly used pump and laser transitions are also given.

Fig. 5.   Transmission mode optical micrograph of the waveguide structures inscribed at (a) 5 MHz repetition rate and ∼30 nJ pulse energy, and (b) 1 MHz repetition rate and similar pulse energies. Both sets are inscribed at sample translation speeds of (left to right) 1, 2, 4, and 8 mm s^{-1}.

earth doped substrates exhibit excellent properties for laser emission. For laser sources for 1 μm, Yb dopant is typically preferred. Ytterbium has a simple energy level scheme with inherently two levels, compared to Neodymium that possess a four level energy system with many possible transitions. Yb systems comprise of $^2F_5/2$ excited state manifold, and $^2F_7/2$ ground state manifold, as shown in Fig. 4. Pumping and laser transitions occur between the various Stark levels of each manifold. For the pumping of Yb^{3+} doped systems, wavelengths ranging from 0.9 μm to 1 μm can be used, with the laser transitions centered just above 1 μm. The higher energy sublevels of the ground state functions as the lower laser level, thereby making the Yb-doped laser systems work as a quasi-three level system. The simple energy level scheme of Yb^{3+} ensures the absence of various detrimental effects such as excited state absorption and cross-relaxation. The lower fluorescence quenching in this system allows high rare earth solubility. Also, the small quantum defect facilitates efficient lasing. A disadvantage that arises in the system is the pump-induced thermal loading that occurs at high pump intensities.

There have been many reports of Yb doped lasers [10], [13], [55]. Yb doped glass systems with their broad luminescence and high rare earth solubility find several applications in science and technology. In telecommunications, they find use in wavelength division multiplexing systems which require broad band amplification. The efficient laser action around 1 μm in Yb doped systems is utilized in bio-medical applications and material processing. Yb doped phosphate glass laser with 90% slope efficiency has been obtained pumped by a 975 nm fiber coupled laser diode [56]. Lasing has also been observed in glass fiber lasers [10], [11], [13], [55]. Waveguide lasers are also of import because of their impact in integrated optical applications. Waveguide architecture provides the advantage of realising more compact and efficient laser sources. These usually have a monolithic laser cavity that can be easily integrated with other optical elements. Many reports have shown devices inscribed in silica based glass, since they can be easily integrated in telecommunication systems. However, the preference for non-silicate host systems have sprung due to the limited amplifier bandwidth and doping concentration of rare earth ions possible in silica glasses [57]. Recently, Bismuthate glass has been studied as a host glass for Yb-dopant ions; for laser applications. Laser action was reported from a highly Yb-doped bismuth ox-
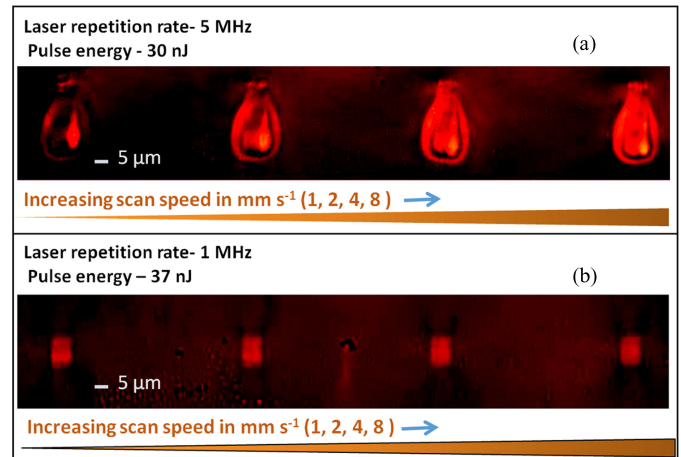
ide based fiber with a slope efficiency of 36% [57]. The study presented below aims to investigate the lasing capabilities of waveguides written in the same glass.

The substrate material used for waveguide fabrication was a Yb-doped Bismuthate glass (Yb-BG) with a dopant concentration of 6600 wt-ppm (1.6×10^{26} m^{-3}). The glass has a refractive index of 2.03, and a peak absorption at a wavelength of 975 nm. To investigate the suitability of the material for ULI, waveguides were written at a range of pulse repetition rates ranging from 200 kHz to 5 MHz and pulse energies between 20 and 120 nJ, and for different sample translation speeds. The polarization of the beam was set to be circular and a 0.4 NA aspheric lens was used to focus the beam ∼200 μm below the sample surface. The multi-scan writing technique was employed to control the waveguide cross-section. For this particular case, we used 20 overlapping laser scans along the sample length, with each scan separated by 0.4 μm along the sample width.

The waveguide morphology was analyzed using a white light microscope working in the transmission mode. All the fabricated waveguides had a brighter contrast compared to the sample substrate, indicating a positive refractive index change. For each laser repetition frequency, the waveguide cross-section exhibited material damage at high pulse energies of the order of ∼100 nJ and lower translation speed of 1 mm s^{-1}. At lower pulse energies (90–40 nJ) and higher translational speeds ∼8 mm s^{-1}, the cross-section modified to tear-drop formation and further modified to square cross-section. The transition from tear-drop structure to symmetric square cross-sections was observed for both decreasing repetition rates at constant pulse energy and vice versa. Fig. 5(a) shows the tear-drop shaped cross-sections of waveguides written at 5 MHz repetition rate, with a sample translation speed of 1, 2, 4, and 8 mm s^{-1}, increasing to the right. The waveguide structure is attributed to the cumulative heating effects characteristic at high repetition rates. 1 MHz laser repetition rate was found to be an optimal inscription parameter, providing close to square waveguide cross-sections as shown in Fig. 5(b).
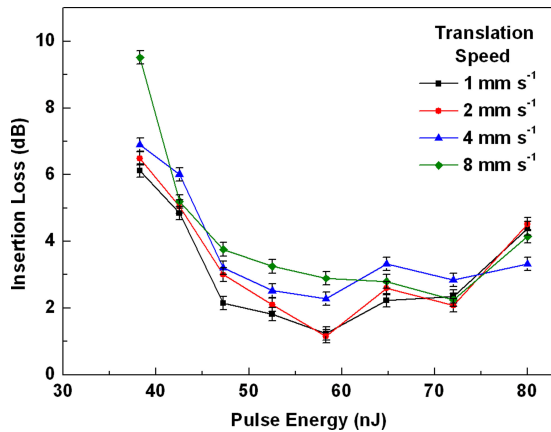
Fig. 6. Insertion loss versus laser pulse energy for waveguides inscribed at 1 MHz laser repetition rate, for different sample translation speeds.
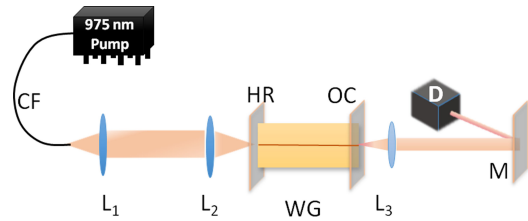

Fig. 7. Schematic of the setup for laser measurements. L1-30X aspheric lens, L2-30X aspheric lens, L3-10X aspheric lenses, CF-coupler fiber, HR-high reflector mirror, WG-waveguide inscribed in Yb-BG, OC-output coupler, M-dichroic mirror, D-detector.
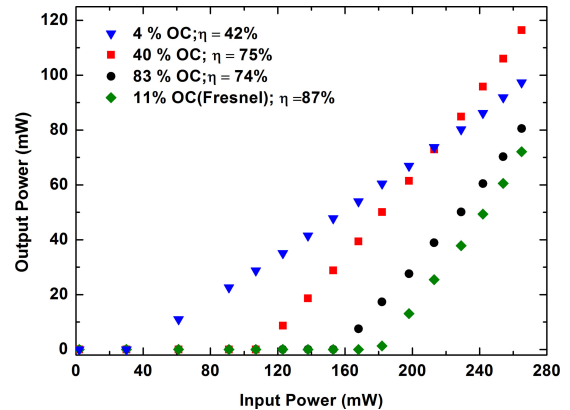

Fig. 8. Evolution of output power with respect to launched pump power, for different output couplers.

The quality of the inscribed waveguides is quantified by measuring the insertion loss (IL). IL is defined as the loss in signal power incurred when a waveguide is inserted into an optical fiber test-bed. IL comprises of coupling losses at the input and output ends of the waveguide, propagation loss within the medium and Fresnel reflections at the interfaces. An Nd:YAG laser at a working wavelength of 1064 nm was chosen for IL measurements in Yb-BG, since the wavelength corresponds to a region of minimal absorption for the sample. The trend of the waveguide insertion loss with respect to pulse energy is given in Fig. 6.

The waveguides written at 1 MHz follow the characteristic trend for ULI waveguides that exhibit smooth refractive index change. At pulse energies greater than ∼70 nJ, the material modification is at the boundary between the regions of pure refractive index modification and that of optical damage. The higher occurrence of scattering and absorption centres at these pulse energies due to thermal diffusion results in a higher insertion loss for the waveguides as observed in Fig. 6. As the pulse energy is lowered, the material modification is manifested as a well defined refractive index modification which results in waveguides with low and comparable losses. At laser pulse energies < 45 nJ, the modification becomes fainter, resulting in weakly guiding structures characterized by higher insertion losses.

For subsequent active measurements, a waveguide in a ∼48.7 mm long Yb-BG sample was used. The waveguide was inscribed with a laser pulse energy of 52 nJ, and translation speed of 8 mm s^{-1}, and measured an IL of 2.4 dB at 1064 nm. Fig. 7 shows the configuration of the laser cavity. A fiber coupled diode laser at 975 nm was used as pump laser. The light from the pump laser was collimated using lens L1 and focused into the laser cavity using lens L2. The sample was placed on a platform with xyz translation control. The laser cavity consisted of the waveguide as the gain medium, and the cavity mirrors butt-coupled to either facet using index matching gel. A dielectric mirror with high transmission at 975 nm, and high reflectivity beyond 1 μm was used as the pump mirror. For the output coupler, a number of partial reflectors for 1064 nm,

with output coupling percentage varying between 3 and 89 were used. The output from the waveguide was collected by lens L3. The dichroic mirror M was used to let the pump beam to pass through while reflecting the collimated signal output at a small angle which is then detected by detector D (KD Optics DATS 01 HP).

Continuous wave (CW) lasing was achieved from the compact integrated cavity using the various output couplers. Fig. 8 gives the evolution of output power with pump for a number of output couplers. The laser with a 4% output coupler has a low pump threshold of 30 mW and a slope efficiency of 42%. With increase in output coupling, the slope efficiency increased almost by a factor of two, at the expense of increased lasing threshold. In the absence of any output coupler, lasing was achieved as a result of the 11% Fresnel reflection at the waveguide output facet. This laser configuration measured a slope efficiency of 87%, close to the quantum defect limit. A steady-state intra-cavity intensity analysis was performed to find the output coupling that guarantees optimum laser performance. The optimal output coupling for the laser was estimated to be 30% [27]. Correspondingly, a maximum output power of 163 mW for 265 mW incident pump power was obtained resulting in an optical conversion efficiency of 62%. The laser has a high slope efficiency of 79%, and a low threshold of 35 mW at an operating wavelength of 1035 nm.

For pulsed laser operation, a SA based output coupler was used, thereby maintaining the compact cavity configuration. Laser performance was investigated using Semiconductor Saturable Output Couplers, CNT and graphene SA. Self-starting
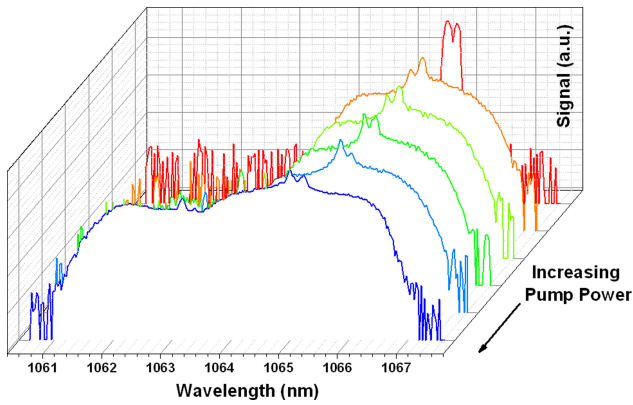
Fig. 9.   Evolution of output spectra with pump power for SOC-1040

Fig. 10.   Pulsed operation using SOC 1060. (a) Q-switched mode-locked pulses. (b) Q-switch envelope. (c) Mode-locked pulse train.

Q-switched mode-locking (QML) was obtained with the SAs. The mode-locked pulses measured a repetition rate of 1.51 GHz in agreement with the cavity length.

Semiconductor saturable output couplers (SOC) combine the principles of the well-known SESAM, and an output coupler; and are available commercially from Batop. The highest available SOC with a fast recovery time has a transmission of ~3%, far from the optimal value of 30%. However, as an initial experiment, we used semiconductor SOCs for the investigation of pulsed operation from the waveguide laser. Initially, a SOC designed for 1040 nm (SOC 1040), with an absorbance of 11%, non-saturable loss of 5% and 6% modulation depth was used. Fig. 9 shows the evolution of the output spectra of the waveguide laser with increase in pump power. The abrupt change from narrow line width CW operation to broad band operation is noticeable, indicative of pulsed operation. Initial studies showed that the working of the laser was hampered by thermal drifts as a result of the high absorbance value of the SOC 1040.

Consequently, a SOC with a low absorption values at the same transmission of 3% was used. Centred at a working wavelength of 1060 nm and hence referred to as SOC 1060 in this paper, the SOC had an absorbance of 2.7%, non-saturable loss of 1% and 1.7% modulation depth. Self-starting QML was observed at a threshold pump power of 53 mW. The mode-locked pulses observed beneath a Q-switch envelope had a repetition rate of 1.5 GHz in accordance with the length of the cavity. The details of the pulsed operation are given in Fig. 10. The laser produced an average output power of 26 mW for a launch pump power of 530 mW, resulting in a low optical conversion efficiency of 5%.

After this first demonstration of pulsed operation from the monolithic waveguide laser, both CNT-SA, and graphene SA were used for a comparative analysis in terms of their lasing threshold, and slope efficiencies. QML operation was obtained for both, with the mode-locked pulses having a repetition rate of 1.51 GHz in agreement with the cavity length.

Using CNT-SA coated on a 40% OC, self-starting QML was initiated at an input pump power of ~130 mW. Fig. 11 gives the rf spectra measured using a Rigol DSA 1030 spectrum analyser showing a fundamental repetition rate of 1.51 GHz. The magnitude spectrum showing the fundamental repetition rate and the harmonics of the pulsed laser, measured using a wide-bandwidth
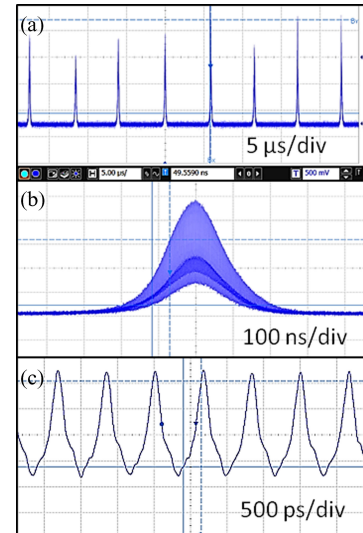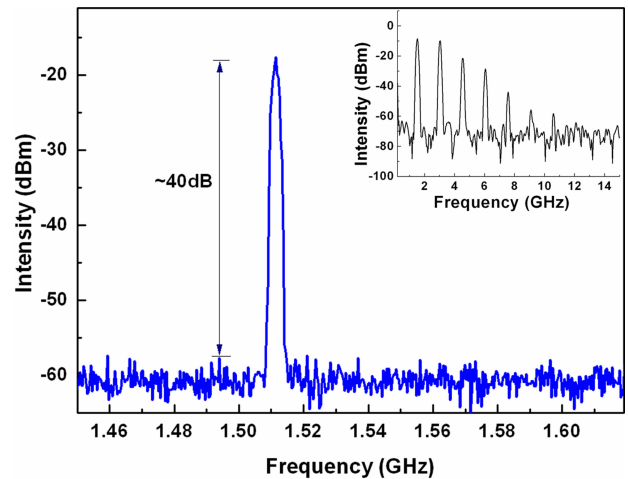

Fig. 11.   RF Spectra of the 1.5 GHz mode-locked pulses observed under a Q-switched envelope using CNT-SA. Inset shows the magnitude spectra with the higher harmonics.

oscilloscope is shown in the inset of the Fig. 11. With increasing pump power, the repetition rate of the Q-switched pulses was found to increase, indicating a tendency towards CW-mode-locking.

The evolution of the average power output from the Fabry-Perot cavity waveguide laser with the CNT-SA, with respect to pump power is given in Fig. 12(a). A maximum output power of 112 mW was obtained for a launched pump power of 530 mW, resulting in an optical conversion efficiency of 21%. The laser has a slope efficiency of 27%.

By replacing CNT with graphene and using a 40% OC, the laser efficiency was found to increase almost by a factor of 2. A threshold pump power of 100 mW was required for self-starting QML. A mode-locked pulse repetition rate of 1.51 GHz was obtained with a Q-switched pulse repetition rate of 0.95 MHz at the maximum pump. Fig. 12(b) shows the evolution of the output power as a function of launched pump. The laser produced
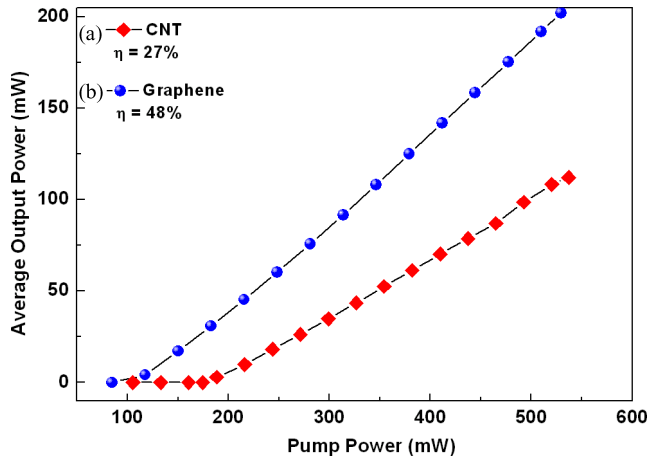
Fig. 12. Output power with launched pump power in (a) (in red) CNT-SA setup, and (b) (in blue) graphene SA setup. The available pump power is 530 mW.

a maximum output power of 202 mW, with a slope efficiency of 48%. The optical spectrum is centred at 1039 nm with a full-width half-maximum (FWHM) spectral bandwidth of 1.1 nm. The pulse duration was measured to be 1.06 ps, The laser pulses had a time-bandwidth product of ~0.324, close to 0.315, expected for bandwidth-limited $sech^2$-shaped pulses [54].

With a view to scale the achievable power from the system and investigate the possibility of attaining continuous-wave mode-locking, we used two 976 nm fiber-coupled diodes. A total pump power of 1 W was available by polarization combining the two outputs into a single fiber. Self-starting QML operation was obtained at a pump threshold of 100 mW. A maximum output of 485 mW was achieved resulting in an optical conversion efficiency of 43%. The laser has a slope efficiency of 49%, as shown in Fig. 13.

For the complete characterization of the high efficiency pulsed waveguide laser, optical saturation experiment for the graphene SA film was performed at 1064 nm. The graphene SA was measured to have a saturation fluence of 10.2 μJ/cm^2, and modulation depth of 17.6% [54]. These values were used to analyse the possibility of obtaining mode-locked pulses with high amplitude stability from the integrated cavity. The criterion for stable CW mode-locking is given as [58]:

$$E_p^2 > E_{L,\text{sat}} E_{A,\text{sat}} \Delta R \qquad (2)$$

where E_p is the intracavity pulse energy and $E_{L,\text{sat}}, E_{A,\text{sat}}$ are the saturation energies of the gain medium and the SA respectively, and ΔR is the modulation depth of the SA. The term on the right is also called as QML parameter. For the Yb-BG glass waveguide laser at its best performance, producing 485 mW, the square of the pulse energy in the cavity was found to be less than the QML parameter, by two orders of magnitude. Therefore, achievement of stable continuous-wave mode-locking using the waveguide requires further engineering of the SA, or a modification in the laser cavity design.

Despite the fact that power scaling is a desirable feature for waveguide lasers, its development inherently follows the same trend as that of fiber lasers, including the detrimental effects. Similar to fiber lasers, the average output power from a wave-
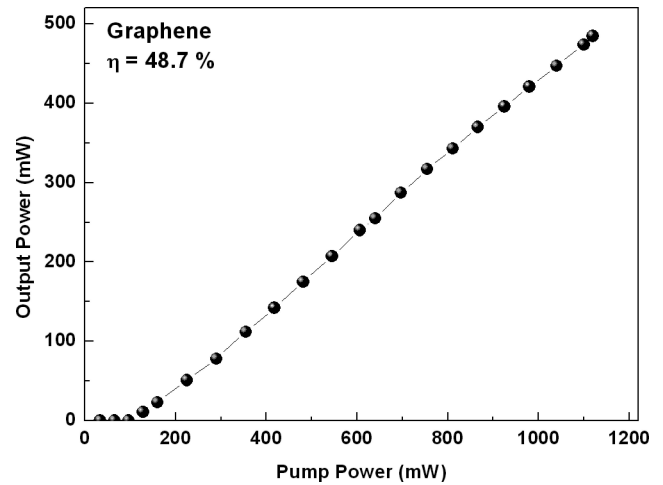

Fig. 13. Evolution of average output power with respect to pump power, in the waveguide laser incorporating graphene SA. The available pump power is ~1 W, resulting in a laser output power of 485 mW and slope efficiency of 50%.
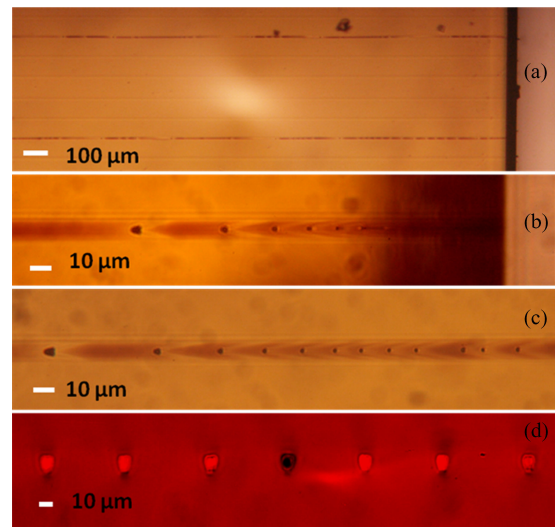

Fig. 14 Optical microscope images showing waveguide damage by fiber-fuse effect. (a) Top surface view of the sample shows two damaged waveguides. (b) A zoomed in top view of the fiber-fuse damage. The input facet of the waveguide is at the right, with the pump light incident from this side. (c) This top surface view gives a clearer image of the observed bullet shaped damage centers in the waveguide core. (d) Comparison of the cross-sectional images of the guiding structures and the waveguide core damaged by fiber fuse.

guide laser is affected by the high nonlinearity in the waveguide cores. Another hampering effect is the fiber-fuse effect. A fiber-fuse is a continuous destruction of the optical fiber core, induced and fed by the propagating light. It is triggered by the local heating of a waveguide structure through which a high power beam is being delivered. Once the heat induced high density plasma is captured in the core region, it travels along the fiber toward the laser source, consuming the light energy and leaving a hollow damage train. For the high-power operation of the Yb-BG waveguide laser mode-locked by graphene, and emitting 485 mW output, a fiber-fuse effect was observed that resulted in complete damage of the waveguide core along the entire length. The effect was characterized by periodic voids and bubble formation, and initiated at the far end of the cavity. Fig. 14(a-c)

shows the images as viewed from the top surface of the waveguide, with the periodic bullet shaped hollow damage centres. Fig. 14(d) shows the damaged waveguide facet in comparison with the neighbouring guiding structures. While this effect is highly undesirable, the demonstration, however accidental, is a clear indication of another issue that needs to be resolved in the path of compact waveguide laser development.

In summary, we have presented the application potential of a single ULI waveguide, facilitated by a highly stable commercial fiber laser system manufactured by IMRA. A compact Fabry-Perot cavity waveguide laser was successfully demonstrated for an operation wavelength around 1 μm, with CW operation resulting in high efficiencies near the quantum defect limit. The same cavity also worked as an efficient ultrafast laser emitting Q-switched mode-locked pulses with a pulse duration of $\sim$1 ps, and the performance features depending on the type of saturable absorber.

B. Selective Etching: Application in Compact Lab-on-a-Chip Devices

When ultrashort (NIR) pulses of typically sub-500 fs duration are focused within the volume of a transparent dielectric material, in addition to inducing refractive index change in the focal volume, the material modification also manifests as a local enhancement of the chemical etching selectivity. This effect enables the fabrication of embedded microfluidic channels within the material that can be monolithically integrated with optical waveguides taking advantage of the arbitrary 3-D flexibility offered by ULI. This advantage along with the possibility of 3-D *in situ* fabrication offers a niche capability in the field of compact lab-on-a-chip (LOC) device development. Selective etching has been observed in glasses including fused silica [59] and photosensitive glass [60] as well as in crystalline materials [61]–[63]. Etching selectivity implies that the laser-modified regions can dissolve significantly faster in an etchant solution compared to the unmodified bulk material. The selectivity depends on both the etchant being used and the material being etched. Silica based glass substrates have been shown to exhibit selective etching in acid (aqueous hydrofluoric acid (HF)) [59], [64] as well as alkali [aqueous potassium hydroxide (KOH)] based etchant solutions [65]. Alkali based etching of silica substrates offers better selectivity, although the etching time is observed to be significantly longer compared to acid based etching. Although there are multiple options with respect to the choice of material for developing ULI enabled LOC applications, fused silica in particular offers unique advantages in this regard such as non-porous nature, hydrophilicity and low autofluorescence. The photo-induced selective etching rates in fused silica is controllable and can be tailored by varying inscription parameters such as the energy and repetition rate of the pulses, and translation speed of the substrate. However, the interest in etching fused silica was driven by the observation of nanograting formation in the inscribed regions. The selective etching phenomenon in fused silica has been subject to extensive evaluation in the recent past. Planar sub-wavelength nanogratings are formed inside the vol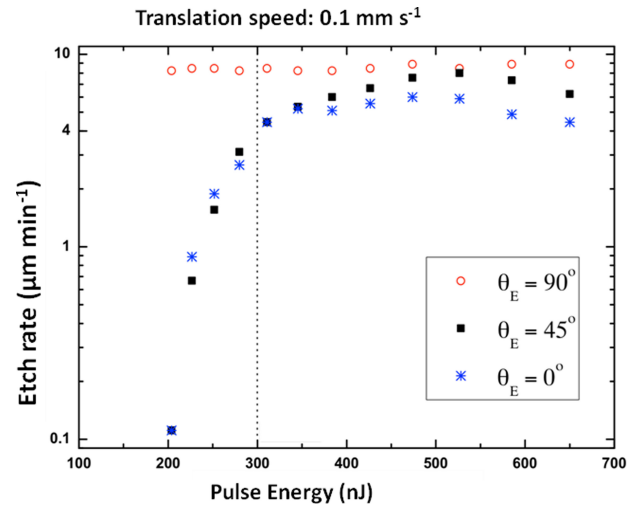ume of fused silica when translated through the focus of linearly polarized pulses and are oriented orthogonal to the electric field vector [21], [66] of the pulses. By rotating the polarization of the incident pulses, the nanogratings can be oriented perpendicular or parallel to the axis of the structure desired for etching. Therefore, the rate of ingress of etchant into the inscribed structure can be controlled by the inscription polarization [67]. Conversely, the observation of etching sensitivity to inscription pulse polarization is indicative of nanograting formation. The nanogratings exhibit long-range order with a periodicity of $\lambda/2n$, where λ is the free-space wavelength and n is the effective refractive index, and appear when the incident pulse energy lies above the maximum threshold for smooth modification and below the minimum threshold for disruptive modification.

Nanograting formation in fused silica was reported to occur for pulse duration lower than approximately 200 fs [21] although more recently evidence of nanograting formation was demonstrated for pulses of duration up to 400 fs [68]. We found evidence of polarisation sensitive etching in fused silica using $\sim$460 fs pulses from the ULI setup shown in Fig. 2 with the repetition rate set at 500 kHz. We studied the etch rate in fused silica with respect to incident pulse energy when the linearly polarized pulses were focused at a depth of 200 μm beneath the surface of a fused silica substrate (Corning, UVFS 7920) using a 0.4 NA aspheric lens. The substrate was translated through the focus for a distance of 4 mm using speeds of 0.1 to 4 mm s^{-1}. Fig. 15 shows the variation of etch rate with respect to pulse energy for a translation speeds of 0.1 mm s^{-1}. The pulse energy was varied from 650 to 200 nJ. Single tracks were inscribed for each pulse energy and translation speed, which were repeated for three cases, wherein the angle between the electric field vector of the inscription pulses and the translation speed direction was maintained at 0°, 90° and 45° as shown in Fig. 16, in order to generate a substantial dataset. The fused silica substrate with the inscribed tracks was then ground back and polished

Fig. 15. Variation of etch rate in fused silica with respect to incident pulse energy using $\sim$460 fs pulses and a translation speed of 0.1 mm s^{-1}. θ_E represents the angle between the electric field vector and translation direction. A clear pulse energy threshold for onset of polarization sensitivity can be observed at $\sim$300 nJ for the etch rate at $\theta_E = 45°$ and $\theta_E = 0°$. No such threshold was observed for $\theta_E = 90°$.
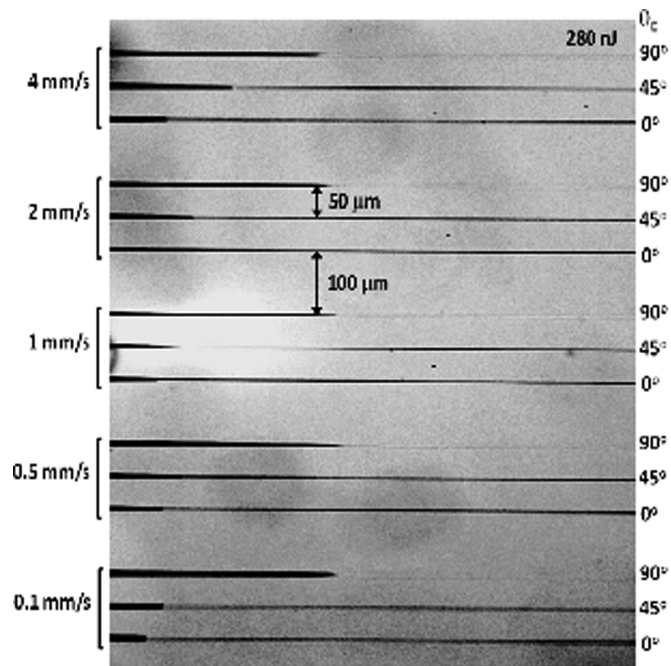
Fig. 16. Bright-field transmission microscope image showing inscribed scans after etching using a 5% (aq.) solution of HF. The pulse energy used to inscribe the scans shown was 280 nJ.
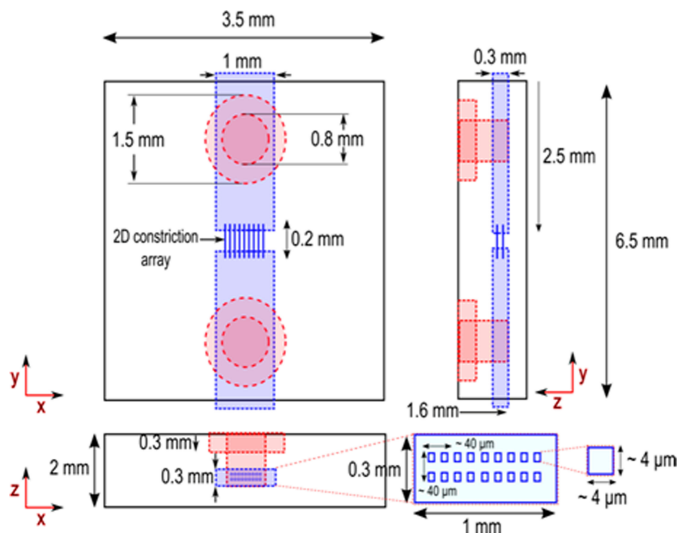

Fig. 17. Schematic representation of the channel and inlet architecture of the device. The channels were designed such that the modified regions extended beyond the frame of the substrate by a short length in order to provide an exit route for un-etched material. Figure is not to scale.

to reveal the facets of the laser-inscribed regions. Etching was subsequently performed using aqueous dilute HF at 5% (v/v) for 45 min.

Similar pulse energy thresholds were observed for the other translation speeds used in this study. The threshold was observed to be $\sim$300 nJ when the translation speed was 0.5 mm s^{-1} and about 380 nJ for translation speeds between 1 and 4 mm s^{-1}. For pulse energies above $\sim$450 nJ, the etch rates were observed to be within the same order of magnitude for all three polarization orientations. The pulse energy threshold was further observed to have insignificant effect on the etch rate of laser written structures when $\theta_E = 90°$.

This observation presents evidence of nanograting formation in laser-inscribed regions within the volume of the fused silica substrate using pulse durations of $\sim$460 fs, which is longer than previous reports. Nanograting formation is a unique feature of ULI as it creates the opportunity to tailor the etch rates of laser inscribed structures, especially for LOC devices where microfluidic structures with large differences in aspect-ratio are often desired. Appropriate manipulation of laser-inscription parameters can enable control over the etch rates for millimeter scale and micrometer scale structures and optimize these to preserve the post-etch aspect-ratio of the structures.

The polarization sensitive etching phenomenon in fused silica was applied in fabricating a LOC device aimed at separating a population of mammalian cells with heterogeneous deformability into sub-populations with uniform degrees of deformability. The device incorporated a 3-D microfluidic channel network embedded within the volume of a 2 mm thick substrate. As shown in Fig. 17, the device architecture comprised of two axially aligned channels that form the input and output sections of

the device. The cross-section of the channels was designed to be 300 μm $\times$ 1 mm with a length of 3.1 mm for both channels. The channels were linked together using a 2-D array of 18 constrictions that was symmetrically aligned across the cross-section of the larger pair of channels with a spacing of 40 μm and a length of 200 μm. Two cylindrical inlet ports were designed to enable fluidic interfacing.

Inscription of the device was performed with a 0.4 NA aspheric lens using 460 fs pulses from the ULI setup described in Fig. 2, which was operated at 500 kHz. The channels were inscribed using 650 nJ pulses at a translation speed of 2 mm s^{-1} while the inlets were inscribed using the same pulse energy at a faster speed of 4 mm s^{-1}. The constrictions were inscribed using 270 nJ pulses at 0.1 mm s^{-1}. The device was subsequently etched using a 13.3% aqueous solution of HF for 4.5 h. The polarization-sensitive etch rates determined using the linear single track inscription mentioned earlier provided the information necessary to ensure balanced etching of the device. Fig. 18 shows the transmission microscope images of the components of the device before (left) and after (right) etching.

The deformability based cell separation was achieved using human promyelocytic leukemia (HL60) cells with an average size of 11.7 μm $\pm$ 1.1 μm. The cell population cultured in DMEM (Life Technologies) was injected into the input channel using a microfluidic syringe infusion pump (WPI, SP100i). Prior to use, the device was primed using phosphate buffered saline. The device was able to successfully operate at flow rates ranging from about 2 μL to 1 mL min^{-1} indicating robust, leak free functioning. The constrictions were found to be of optimum cross-section to enable deformation of the cells during transit and exhibited asymmetric post-etch dimensions of 4 and 8 μm along the short and long axis respectively. The device was found to exhibit a throughput of $\sim$3000 cells min^{-1}. The integrity of the cell membrane for the device output population was analyzed by performing a live-dead analysis using a commercial flow
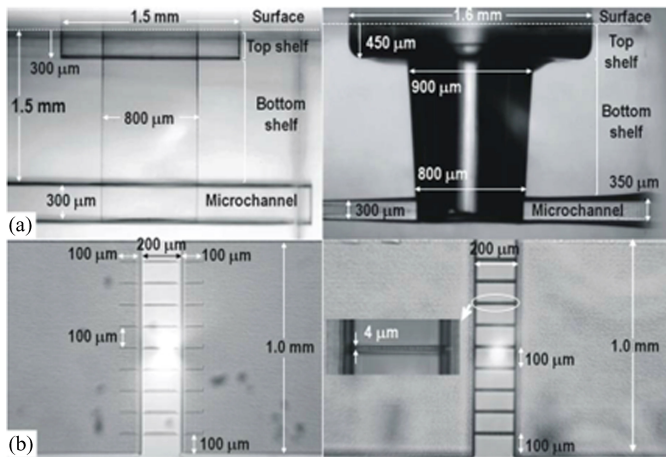
Fig. 18.   Transmission microscope images showing the components of the device before (left) and after (right) etching. Reproduced from ref [28] with permission from The Royal Society of Chemistry.
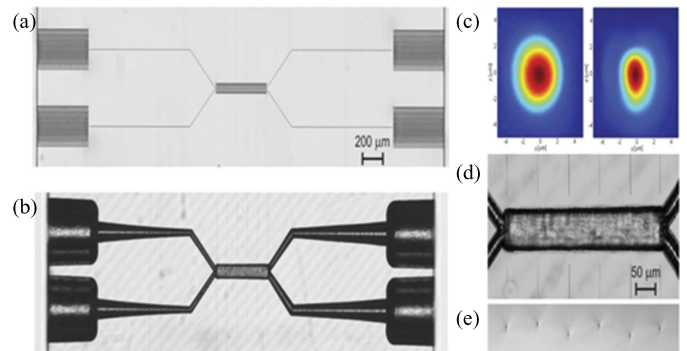

Fig. 19.   (a) Microscope image of the femtosecond laser irradiation pattern to form the integrated optical sorter. (b) Same structure shown in (a) after 5 h of chemical etching in 20% aqueous solution of HF; the central common branch is 0.5 mm long. (c) Intensity mode profile at 1 μm wavelength of (left) optical fiber and (right) femtosecond laser written waveguide. (d) Microscope image of the central common branch of the sorter after etching, with facing integrated optical waveguides. (e) Cross-sectional microscope image of fabricated waveguides at different depths. Reproduced from [70] with permission from The Royal Society of Chemistry.

cytometer (BD FACS Calibur). The analysis revealed >80% of the cells collected at the output remained viable. This result offers a simple, label-free separation mechanism based exclusively on cell deformability with promising implications for cellular diagnostic and therapeutic applications. In particular, there is preliminary evidence that human pluripotent stem cells, which are known to be remarkably deformable, progressively become stiffer with the degree of differentiation [69]. The mode of separation demonstrated by the ULI device underscores its potential in fractionating a population of differentiated cells based on their degree of deformability.

The 3-D monolithic integration of embedded microfluidic channels with NIR optical waveguides is a unique capability offered by the ULI technique. An elegant application of this capability was recently demonstrated in a waveguide enabled, fluorescence-activated cell-sorting device in fused silica [70]. The device design included an X-shaped channel where two input channels merge in a central section, in which fluorescence investigation and sorting are performed. This section then separates into two output channels as shown in Fig. 19.

The frequency doubled output from a 1040 nm regeneratively amplified commercial laser (femtoREGEN, HIGHQlaser) delivering ≥400 fs pulses and operating at 500 kHz was used to fabricate the device. A 50 × 0.6 NA microscope objective was used as the focusing optic. The microchannel was inscribed using a second-harmonic pulse energy of 700 nJ and a translation speed of 1 mm s^{-1} at a depth of 400 μm beneath the surface. The optical waveguides were inscribed using 100 nJ pulses at a translation speed of 0.1 mm s^{-1}, the parameters for which were separately optimized for guiding at 1 μm. Selective etching was subsequently performed by immersing the laser modified fused silica substrate in a 20% aqueous solution of HF at a slightly elevated temperature of 35 °C in an ultrasonic bath. The device was designed to work with fluorescent as well as non-fluorescent samples. A continuous wave beam from a Yb fibre laser capable of generating 5 W optical power at 1070 nm was launched into a waveguide designated for use as a light source to exert radiation pressure on the particle to be sorted. Additionally, on the side

closer to the input end of the chip, a 532 nm or 473 nm wavelength laser, depending upon the fluorophore excitation wavelength, was coupled to an optical waveguide designated to excite fluorescence when polystyrene fluorescent beads or fluorescent cells flowed in the microchannels respectively. Fluorescence detection was used to automatically trigger the sorting waveguide which when turned on, exerted radiation pressure on the target entity to enable its flow along the desired microchannel arm. The device was capable of sorting a cell sample comprising human transformed fibroblasts transfected with a plasmid encoding the enhanced green fluorescent protein (eGFP).

The application of ULI in developing compact LOC devices has evolved rapidly in the past decade from being purely exploratory into an accomplished technology capable of addressing niche demands in the field such as 3-D *in situ* fabrication and monolithic integration capabilities. It is envisaged that future development in optimized fabrication schemes for low-loss photonic components and microfluidic structures with improved selectivity in chemical etching will lead to the emergence of high-quality 2-D and 3-D optofluidic architectures.

V. SUMMARY AND CONCLUSION

The field of rare earth doped fiber lasers has witnessed unprecedented advances and is now an integral part of many photonic applications including biomedicine, material processing, astronomy and fundamental research. Fiber lasers have an extremely robust laser design with diffraction limited beam quality and can produce high average output powers. Continuous wave fiber lasers with output powers above 1 kW are now available. The advances in this field have also resulted in pulsed fiber lasers with high pulse energies and short pulse durations. Fiber laser development still remains an active field of research, aiming towards the development of more robust, high power systems that in turn promote scientific research and further commercialization.

The immense development in the field of fiber lasers and its vast scope is reflected in the unparalleled advances in its application regimes. The high stability, high pulse energy and short pulse durations of fiber lasers have revolutionized laser material processing. In terms of micromachining of transparent materials alone, fiber lasers has allowed the investigation of material processing over a wider parameter range for a large number of substrates. The stability of the laser provides higher productivity and repeatability for ULI. ULI waveguide based passive, and active photonic devices, and optofluidic devices have now transformed the outlook for integrated optical applications, even leading to commercialization of ULI devices [71].

REFERENCES

[1] E. Snitzer, "Optical maser action of Nd+3 in a barium crown glass," *Phys. Rev. Lett.*, vol. 7, pp. 444–446, 1961.

[2] E. Snitzer, F. Hoffman, and R. Crevier, "Neodymium-glass-fiber laser," *J. Opt. Soc. Amer.*, vol. 53, pp. 515–517, 1963.

[3] R. J. Mears, L. Reekie, S. B. Poole, and D. N. Payne, "Neodymium-doped silica single-mode fiber lasers," *Electron. Lett.*, vol. 21, pp. 738–740, 1985.

[4] T. Eidam, S. Hanf, E. Seise, T. V. Andersen, T. Gabler, C. Wirth, T. Schreiber, J. Limpert, and A. Tunnermann, "Femtosecond fiber CPA system emitting 830 W average output power," *Opt. Lett.*, vol. 35, pp. 94–96, 2010.

[5] Y. Jeong, J. K. Sahu, D. N. Payne, and J. Nilsson, "Ytterbium-doped large-core fibre laser with 1 kW of continuous-wave output power," *Electron. Lett.*, vol. 40, pp. 470–472, 2004.

[6] T. Erdogan, "Fiber grating spectra," *J. Lightw. Technol.*, vol. 15, no. 8, pp. 1277–1294, Aug. 1997.

[7] J. Limpert, F. Roser, T. Schreiber, and A. Tunnermann, "High-power ultrafast fiber laser systems," *IEEE J. Sel. Topics Quantum*, vol. 12, no. 2, pp. 233–244, Mar./Apr. 2006.

[8] R. Kashyap, "The Fiber Fuse - from a curious effect to a critical issue: A 25th year retrospective," *Opt. Exp.*, vol. 21, pp. 6422–6441, 2013.

[9] B. Samson, A. Carter, and K. Tankala, "Doped Fibers: Rare-earth fibres power up," *Nat. Photon.*, vol. 5, pp. 466–467, 2011.

[10] A. Chong, J. Buckley, W. Renninger, and F. Wise, "All-normal-dispersion femtosecond fiber laser," *Opt. Exp.*, vol. 14, pp. 10095–10100, 2006.

[11] A. Chong, W. H. Renninger, and F. W. Wise, "All-normal-dispersion femtosecond fiber laser with pulse energy above 20 nJ," *Opt. Lett.*, vol. 32, pp. 2408–2410, 2007.

[12] U. Keller, "Ultrafast solid-state laser oscillators: A success story for the last 20 years with no end in sight," *Appl. Phys. B, Lasers O*, vol. 100, pp. 15–28, 2010.

[13] L. A. Gomes, L. Orsila, T. Jouhti, and O. G. Okhotnikov, "Picosecond SESAM-based ytterbium mode-locked fiber lasers," *IEEE J. Sel. Topics Quantum*, vol. 10, no. 1, pp. 129–136, Jan./Feb. 2004.

[14] S. Yamashita, "A Tutorial on nonlinear photonic applications of carbon nanotube and graphene," *J. Lightw. Technol.*, vol. 30, no. 4, pp. 427–447, Feb. 2012.

[15] G. K. Moeller, "10.6 Micron carbon dioxide laser with helium added," US 3464028 A, Perkin Elmer Corp., Waltham, MA, USA, 1969.

[16] G. Kamlage, T. Bauer, A. Ostendorf, and B. N. Chichkov, "Deep drilling of metals by femtosecond laser pulses," *Appl. Phys. A, Mater.*, vol. 77, pp. 307–310, 2003.

[17] A. Schoonderbeek, V. Schutz, O. Haupt, and U. Stute, "Laser processing of thin films for photovoltaic applications," *J. Laser Micro. Nanoen.*, vol. 5, pp. 248–255, 2010.

[18] R. R. Gattass and E. Mazur, "Femtosecond laser micromachining in transparent materials," *Nat. Photon.*, vol. 2, pp. 219–225, 2008.

[19] K. M. Davis, K. Miura, N. Sugimoto, and K. Hirao, "Writing waveguides in glass with a femtosecond laser," *Opt. Lett*, vol. 21, pp. 1729–1731, 1996.

[20] C. B. Schaffer, A. Brodeur, and E. Mazur, "Laser-induced breakdown and damage in bulk transparent materials induced by tightly focused femtosecond laser pulses," *Meas. Sci. Technol.*, vol. 12, pp. 1784–1794, 2001.

[21] R. Taylor, C. Hnatovsky, and E. Simova, "Applications of femtosecond laser induced self-organized planar nanocracks inside fused silica glass," *Laser Photon. Rev*, vol. 2, pp. 26–46, 2008.

[22] B. C. Stuart, M. D. Feit, S. Herman, A. M. Rubenchik, B. W. Shore, and M. D. Perry, "Optical ablation by high-power short-pulse lasers," *J. Opt. Soc. Amer. B*, vol. 13, pp. 459–468, 1996.

[23] Y. Bellouard and M. O. Hongler, "Femtosecond-laser generation of self-organized bubble patterns in fused silica," *Opt. Exp.*, vol. 19, pp. 6807–6821, 2011.

[24] C. B. Schaffer, A. O. Jamison, and E. Mazur, "Morphology of femtosecond laser-induced structural changes in bulk transparent materials," *Appl. Phys. Lett.*, vol. 84, pp. 1441–1443, 2004.

[25] E. N. Glezer and E. Mazur, "Ultrafast-laser driven micro-explosions in transparent materials," *Appl. Phys. Lett.*, vol. 71, pp. 882–884, 1997.

[26] L. Sudrie, M. Franco, B. Prade, and A. Mysyrowicz, "Study of damage in fused silica induced by ultra-short IR laser pulses," *Opt. Commun.*, vol. 191, pp. 333–339, 2001.

[27] R. Mary, S. J. Beecher, G. Brown, R. R. Thomson, D. Jaque, S. Ohara, and A. K. Kar, "Compact, highly efficient ytterbium doped bismuthate glass waveguide laser," *Opt. Lett.*, vol. 37, pp. 1691–1693, 2012.

[28] D. Choudhury, W. T. Ramsay, R. Kiss, N. A. Willoughby, L. Paterson, and A. K. Kar, "A 3D mammalian cell separator biochip," *Lab Chip*, vol. 12, pp. 948–953, 2012.

[29] G. Brown, R. R. Thomson, A. K. Kar, N. D. Psaila, and H. T. Bookey, "Ultrafast laser inscription of Bragg-grating waveguides using the multiscan technique," *Opt. Lett.*, vol. 37, pp. 491–493, 2012.

[30] S. J. Beecher, R. R. Thomson, N. D. Psaila, Z. Sun, T. Hasan, A. G. Rozhin, A. C. Ferrari, and A. K. Kar, "320 fs pulse generation from an ultrafast laser inscribed waveguide laser mode-locked by a nanotube saturable absorber," *Appl. Phys. Lett.*, vol. 97, pp. 111114-1–111114-3, 2010.

[31] Y. Bellouard, A. A. Said, and P. Bado, "Integrating optics and micromechanics in a single substrate: A step toward monolithic integration in fused silica," *Opt. Exp.*, vol. 13, pp. 6635–6644, 2005.

[32] R. R. Thomson, N. D. Psaila, S. J. Beecher, and A. K. Kar, "Ultrafast laser inscription of a high-gain Er-doped bismuthate glass waveguide amplifier," *Opt. Exp.*, vol. 18, pp. 13212–13219, 2010.

[33] R. Osellame, N. Chiodo, G. della Valle, S. Taccheo, R. Ramponi, G. Cerullo, A. Killi, U. Morgner, M. Lederer, and D. Kopf, "Optical waveguide writing with a diode-pumped femtosecond oscillator," *Opt. Lett.*, vol. 29, pp. 1900–1902, 2004.

[34] R. R. Thomson, N. D. Psaila, H. T. Bookey, D. T. Reid, and A. K. Kar, "Controlling the cross-section of ultrafast laser inscribed optical waveguides," in *Femtosecond Laser Micromachining, Topics in Applied Physics*. vol. 123, Berlin, Germany: Springer, 2012, pp. 93–125.

[35] C. Hnatovsky, R. S. Taylor, E. Simova, P. P. Rajeev, D. M. Rayner, V. R. Bhardwaj, and P. B. Corkum, "Fabrication of microchannels in glass using focused femtosecond laser radiation and selective chemical etching," *Appl. Phys. A, Mater.*, vol. 84, pp. 47–61, 2006.

[36] J. W. Chan, T. Huser, S. Risbud, and D. M. Krol, "Structural changes in fused silica after exposure to focused femtosecond laser pulses," *Opt. Lett.*, vol. 26, pp. 1726–1728, 2001.

[37] J. W. Chan, T. R. Huser, S. H. Risbud, and D. M. Krol, "Modification of the fused silica glass network associated with waveguide fabrication using femtosecond laser pulses," *Appl. Phys. A, Mater.*, vol. 76, pp. 367–372, 2003.

[38] P. Dekker, M. Ams, G. D. Marshall, D. J. Little, and M. J. Withford, "Annealing dynamics of waveguide Bragg gratings: Evidence of femtosecond laser induced colour centres," *Opt. Exp.*, vol. 18, pp. 3274–3283, 2010.

[39] A. Kubota, M. J. Caturla, J. S. Stolken, and M. D. Feit, "Densification of fused silica due to shock waves and its implications for 351 nm laser induced damage," *Opt. Exp.*, vol. 8, pp. 611–616, 2001.

[40] V. R. Bhardwaj, E. Simova, P. B. Corkum, D. M. Rayner, C. Hnatovsky, R. S. Taylor, B. Schreder, M. Kluge, and J. Zimmer, "Femtosecond laser-induced refractive index modification in multicomponent glasses," *J. Appl. Phys.*, vol. 97, pp. 083102-1–083102-9, 2005.

[41] J. R. Macdonald, S. J. Beecher, P. A. Berry, K. L. Schepler, and A. K. Kar, "Compact mid-infrared Cr:ZnSe channel waveguide laser," *Appl. Phys. Lett.*, vol. 102, pp. 161110-1–161110-3, 2013.

[42] J. R. Macdonald, S. J. Beecher, P. A. Berry, G. Brown, K. L. Schepler, and A. K. Kar, "Efficient mid-infrared Cr:ZnSe channel waveguide laser operating at 2486 nm," *Opt. Lett.*, vol. 38, pp. 2194–2196, 2013.

[43] Y. Tan, A. Rodenas, F. Chen, R. R. Thomson, A. K. Kar, D. Jaque, and Q. M. Lu, "70% slope efficiency from an ultrafast laser-written Nd:GdVO4 channel waveguide laser," *Opt. Exp.*, vol. 18, pp. 24994–24999, 2010.

[44] Y. Y. Ren, G. Brown, A. Rodenas, S. Beecher, F. Chen, and A. K. Kar, "Mid-infrared waveguide lasers in rare-earth-doped YAG," *Opt. Lett.*, vol. 37, pp. 3339–3341, 2012.

[45] J. A. Dharmadhikari, R. Bernard, A. K. Bhatnagar, D. Mathur, and A. K. Dharmadhikari, "Axicon-based writing of waveguides in BK7 glass," *Opt. Lett.*, vol. 38, pp. 172–174, 2013.

[46] R. Osellame, S. Taccheo, M. Marangoni, R. Ramponi, P. Laporta, D. Polli, S. De Silvestri, and G. Cerullo, "Femtosecond writing of active optical waveguides with astigmatically shaped beams," *J. Opt. Soc. Amer. B*, vol. 20, pp. 1559–1567, 2003.

[47] M. Ams, G. D. Marshall, D. J. Spence, and M. J. Withford, "Slit beam shaping method for femtosecond laser direct-write fabrication of symmetric waveguides in bulk glasses," *Opt. Exp.*, vol. 13, pp. 5676–5681, 2005.

[48] R. R. Thomson, A. S. Bockelt, E. Ramsay, S. Beecher, A. H. Greenaway, A. K. Kar, and D. T. Reid, "Shaping ultrafast laser inscribed optical waveguides using a deformable mirror," *Opt. Exp.*, vol. 16, pp. 12786–12793, 2008.

[49] P. S. Salter, A. Jesacher, J. B. Spring, B. J. Metcalf, N. Thomas-Peter, R. D. Simmonds, N. K. Langford, I. A. Walmsley, and M. J. Booth, "Adaptive slit beam shaping for direct laser written waveguides," *Opt. Lett.*, vol. 37, pp. 470–472, 2012.

[50] Y. Nasu, M. Kohtoku, and Y. Hibino, "Low-loss waveguides written with a femtosecond laser for flexible interconnection in a planar light-wave circuit," *Opt. Lett.*, vol. 30, pp. 723–725, 2005.

[51] G. D. Valle, S. Taccheo, R. Osellame, A. Festa, G. Cerullo, and P. Laporta, "1.5 μ m single longitudinal mode waveguide laser fabricated by femtosecond laser writing," *Opt. Exp.*, vol. 15, pp. 3190–3194, 2007.

[52] N. D. Psaila, R. R. Thomson, H. T. Bookey, A. K. Kar, N. Chiodo, R. Osellame, G. Cerullo, A. Jha, and S. Shen, "Er: Yb-doped oxyfluoride silicate glass waveguide amplifier fabricated using femtosecond laser inscription," *Appl. Phys. Lett.*, vol. 90, pp. 131102-1–131102-3, 2007.

[53] Y. Sikorski, A. A. Said, P. Bado, R. Maynard, C. Florea, and K. A. Winick, "Optical waveguide amplifier in Nd-doped glass written with near-IR femtosecond laser pulses," *Electron. Lett.*, vol. 36, pp. 226–227, 2000.

[54] R. Mary, G. Brown, S. J. Beecher, F. Torrisi, S. Milana, D. Popa, T. Hasan, Z. P. Sun, E. Lidorikis, S. Ohara, A. C. Ferrari, and A. K. Kar, "1.5 GHz picosecond pulse generation from a monolithic waveguide laser with a graphene-film saturable output coupler," *Opt. Exp.*, vol. 21, pp. 7943–7950, 2013.

[55] L. Orsila, L. A. Gomes, N. Xiang, T. Jouhti, and O. G. Okhotnikov, "Mode-locked ytterbium fiber lasers," *Appl. Opt.*, vol. 43, pp. 1902–1906, 2004.

[56] D. Jaque, J. C. Lagomacini, C. Jacinto, and T. Catunda, "Continuous-wave diode-pumped Yb: Glass laser with near 90% slope efficiency," *Appl. Phys. Lett.*, vol. 89, pp. 121101-1–121101-3, 2006.

[57] S. Ohara and Y. Kuroiwa, "Highly ytterbium-doped bismuth-oxide-based fiber," *Opt. Exp.*, vol. 17, pp. 14104–14108, 2009.

[58] C. Honninger, R. Paschotta, F. Morier-Genoud, M. Moser, and U. Keller, "Q-switching stability limits of continuous-wave passive mode locking," *J. Opt. Soc. Amer. B.*, vol. 16, pp. 46–56, 1999.

[59] A. Marcinkevicius, S. Juodkazis, M. Watanabe, M. Miwa, S. Matsuo, H. Misawa, and J. Nishii, "Femtosecond laser-assisted three-dimensional microfabrication in silica," *Opt. Lett.*, vol. 26, pp. 277–279, 2001.

[60] K. Sugioka, Y. Hanada, and K. Midorikawa, "Three-dimensional femtosecond laser micromachining of photosensitive glass for biomicrochips," *Laser Photon. Rev*, vol. 4, pp. 386–400, 2010.

[61] S. Matsuo, Y. Tabuchi, T. Okada, S. Juodkazis, and H. Misawa, "Femtosecond laser assisted etching of quartz: microstructuring from inside," *Appl. Phys. A, Mater.*, vol. 84, pp. 99–102, 2006.

[62] D. Choudhury, A. Rodenas, L. Paterson, F. Diaz, D. Jaque, and A. K. Kar, "Three-dimensional microstructuring of yttrium aluminum garnet crystals for laser active optofluidic applications," *Appl. Phys. Lett.*, vol. 103, pp. 041101-1–041101-4, 2013.

[63] D. Wortmann, J. Gottmann, N. Brandt, and H. Horn-Solle, "Micro- and nanostructures inside sapphire by fs-laser irradiation and selective etching," *Opt. Exp.*, vol. 16, pp. 1517–1522, 2008.

[64] Y. Bellouard, A. Said, M. Dugan, and P. Bado, "Fabrication of high-aspect ratio, micro-fluidic channels and tunnels using femtosecond laser pulses and chemical etching," *Opt. Exp.*, vol. 12, pp. 2120–2129, 2004.

[65] S. Kiyama, S. Matsuo, S. Hashimoto, and Y. Morihira, "Examination of etching agent and etching mechanism on femtosecond laser microfabrication of channels inside vitreous silica substrates," *J. Phys. Chem. C*, vol. 113, pp. 11560–11566, 2009.

[66] Y. Shimotsuma, P. G. Kazansky, J. R. Qiu, and K. Hirao, "Self-organized nanogratings in glass irradiated by ultrashort light pulses," *Phys. Rev. Lett*, vol. 91, pp. 247405-1–247405-4, 2003.

[67] C. Hnatovsky, R. S. Taylor, E. Simova, V. R. Bhardwaj, D. M. Rayner, and P. B. Corkum, "Polarization-selective etching in femtosecond laser-assisted microfluidic channel fabrication in fused silica," *Opt. Lett.*, vol. 30, pp. 1867–1869, 2005.

[68] S. Richter, C. Miese, S. Doring, F. Zimmermann, M. J. Withford, A. Tunnermann, and S. Nolte, "Laser induced nanogratings beyond fused silica—Periodic nanostructures in borosilicate glasses and ULE (TM)," *Opt. Mater. Exp.*, vol. 3, pp. 1161–1166, 2013.

[69] R. Kiss, H. Bock, S. Pells, E. Canetta, A. K. Adya, A. J. Moore, P. De Sousa, and N. A. Willoughby, "Elasticity of human embryonic stem cells as determined by atomic force microscopy," *J. Biomech. Eng.*, vol. 133, pp. 101009-1–101009-9, 2011.

[70] F. Bragheri, P. Minzioni, R. M. Vazquez, N. Bellini, P. Paie, C. Mondello, R. Ramponi, I. Cristiani, and R. Osellame, "Optofluidic integrated cell sorter fabricated by femtosecond lasers," *Lab Chip*, vol. 12, pp. 3779–3784, 2012.

[71] Optoscribe. [Online]. Available: http://optoscribe.com/, accessed on 12 Feb. 2014.

Rose Mary received the M.Sc. degree in photonics from the Cochin University of Science and Technology, India, in 2010. She is currently working toward the Ph.D. degree in physics at Heriot-Watt University, Edinburgh, U.K. Her research interests include ultrafast laser inscribed compact waveguide laser sources.

Debaditya Choudhury received the B.Sc. (Hons.) degree in physics from St. Edmund's College, India, in 2002, the M.Sc. degree in physics from the Indian Institute of Technology, Guwahati, in 2005, the M.Sc. degree in forensic materials from Heriot-Watt University, Edinburgh, U.K., where he received the Ph.D. degree in physics in 2013. He is currently a Research Associate in the Photonics Instrumentation Group, Heriot-Watt University. His research interests include ultrafast laser inscribed photonic instruments for microfluidic and astrophotonic applications.

Ajoy K. Kar developed his interest in lasers and nonlinear optics during his PhD at the University of Essex, following his MSc studies at Delhi. He joined Heriot-Watt University in Scotland as a post-doc in 1979, where at present, he is a professor at the Institute of Photonics and Quantum Sciences. His current projects involve amplifiers for telecommunications, ultrafast laser inscription (ULI) for novel optoelectronic device applications, generation of white light continuum from visible to mid-infrared part of the spectrum, and the development of ULI based microfluidic devices for biophotonics applications. He has pioneered Photonics Education in the UK and Europe. Prof. Kar is a member of the Institute of Electrical and Electronics Engineers, and the Optical Society of America.